Desalination and Water Treatment
www.deswater.com

doi: 10.5004/dwt.2020.25349

187 (2020) 219–231
May

Native clay, $MnFe_2O_4$/clay composite and bio-composite efficiency for the removal of synthetic dye from synthetic solution: column versus batch adsorption studies

Sana Nausheen[a,b], Haq Nawaz Bhatti[a,*], Khalid Arif[c], Jan Nisar[d], Munawar Iqbal[e,*]

[a]*Environmental and Material Chemistry Laboratory, Department of Chemistry, University of Agriculture, Faisalabad 38040, Pakistan, hnbhatti2005@yahoo.com (H.N. Bhatti)*
[b]*Department of Chemistry, Government College Women University, Faisalabad, Pakistan*
[c]*Department of Mathematics and Statistics, University of Lahore, Lahore 53700, Pakistan*
[d]*National Centre of Excellence in Physical Chemistry, University of Peshawar, Peshawar 25120, Pakistan*
[e]*Department of Chemistry, The University of Lahore, Lahore 53700, Pakistan, email: munawar.iqbal@chem.uol.edu.pk (M. Iqbal)*

Received 2 September 2019; Accepted 10 December 2019

ABSTRACT

The Blue XGRRL dye removal efficiency native clay, $MnFe_2O_4$/clay composite, and biocomposite were studied. The adsorbent was characterized by X-ray diffraction and Fourier-transform infrared spectroscopy techniques. Affecting process variables, that is, temperature, pH, composite dose, initial concentration of dye and contact time were studied for enhanced dye removal. It was observed that pH 6–9, 0.05 g adsorbent dosage, 30 min contact time, 200 mg/L dye initial concentration at low temperature were the viable conditions for maximum adsorptive removal (49.93 mg/g) of dye. Langmuir isotherm along pseudo-second-order kinetic model fitted well to the dye adsorption data. Thermodynamic study revealed that the adsorption phenomenon was more viable at low temperatures as shown by lower $\Delta G°$ values. The $\Delta H°$ indicated the exothermic adsorption process of Blue XGRRL dye on to composites. Column bed height, Blue XGRRL dye initial concentration, and flow rate were studied in a column adsorption mode and it was observed that higher bed height, higher initial dye concentrations and low flow rates were observed to be more complimentary conditions for efficient adsorptive removal of dye in the column mode. Clay composite's efficiency was significantly higher vs. biocomposite that could be employed for the adsorptive removal of dyes from wastewater.

Keywords: Blue XGRRL; Adsorption; Clay composites; Biocomposite; Equilibrium modeling, Kinetics; Thermodynamics

1. Introduction

Industrialization is one of the main sources of water contamination and environmental pollution. In recent years, water contamination has become an alarming environmental dilemma and has engrossed global attention, particularly since diverse contaminants are entering into the aquatic systems. Dyes are extensively utilized in cosmetics, plastics, food, paper, leather, textile, and pharmaceutical industries. The pollution is mainly caused by effluents from these industries. The presence of dye causes damage to aquatic life because dyes in water bodies preclude the light and aquatic life affected badly and imposed a negative impact on living creatures [1–4]. Mostly the dyes are resistant to biodegradation and photodegradation for the remediation of dyes [5–9]. Therefore, the treatment of wastewater contains dye need efficient techniques to avoid the environmental issue [3,10–12].

Various treatment approaches have been utilized for the sequestration of contaminants from effluents. Adsorption is considered as one of the viable technique vs. other techniques such as biodegradation and photodegradation [9,13–25].

* Corresponding authors.

Adsorption offers various, that is, flexibility, low operation cost, uncomplicated devise, ease in operation, lack of sensitivity for toxic contaminants, easy automation and the ability to operate at a very low concentration of pollutants [1,2,4,26]. Adsorption uses inexpensive adsorbents, which become a feasible option for the adsorptive removal of dyes due to their cost-effective, regeneration possibility of the adsorbent, abundantly available and opportunity of recovery. Adsorbents of smaller particle size not only increase effective surface area but also enhance mass transfer efficacy [27–30].

Among the cost-effective materials, clays are natural, inexpensive and abundant materials that have an exclusive layered structure, good chemical resistance as well as high mechanical strength [31–34]. Studies have shown that clays are good adsorbents for the adsorptive removal of dyes from textile effluents. To date, the modified adsorbents have been prepared and employed successfully for the adsorptive removal of pollutants and composite materials showed a promising affinity for the adsorption of pollutants from wastewater [2,35,36]. Owing to the high reactivity and selectivity towards specific contaminants, the composites are proved too attractive an alternative for the adsorptive removal of pollutants from wastewater [13,14,16,28–30,37].

Based on the aforementioned facts, the present research was focused on the preparation of clay composite and biocomposite. The prepared composites were compared for the adsorptive removal of Blue XGRRL dye both in batch and column adsorption modes. For batch mode, the process variables, that is, temperature, Blue XGRRL dye initial concentration, pH, contact time and composite dose were optimized for maximum dye removal, whereas in column bed height, initial dye concentration and flow rate were optimized. The equilibrium, kinetic and thermodynamic studies were also performed for both types of the adsorbent for the evaluation of adsorption nature of dye on to composites.

2. Materials and methods

2.1. Chemicals and biomass preparation

The chemicals and reagents used were of analytical grade and used without any purification. The natural clay was obtained from Khoshab, Pakistan. The rice bran, sunflower, cotton sticks, sugarcane bagasse, corn cobs, and peanut hulls biomasses were collected from different areas of Faisalabad, Punjab, Pakistan. Biomasses were washed water, dried in sunlight and overnight at 60°C in the oven.

2.2. Preparation of clay composites

The co-precipitation method was adopted for composites preparation. For this, clay (10 g) was mixed thoroughly with $MnCl_2$ and $FeCl_3$ (Equal ratio). The pH adjusted to 10 using NH_4OH and the mixture was stirred for 30 min followed by heating for 2 h at 95°C. The composite was washed with water (thrice) and dried for 2 h at 105°C [38].

2.3. Preparation of biocomposites

Among, all biomasses screened for dye adsorption, the peanut hulls showed higher efficient and this biocomposite was used in subsequent studies. For this, a slurry of clay with the biomass was prepared with a 1:1 ratio. The mass thus obtained kept for 24 h at 60°C, ground and sieved using 300 μm OCT-DIGITAL 4527-01 siever.

2.4. Batch experimental program

Blue XGRRL was obtained from Faisalabad, Pakistan (local supplier). The dye stock solution (1 g/L) was prepared double distilled water and working concentrations (25–400 mg/L) were prepared by dilution. Batch experiments were performed for the comparison of adsorption capacity of clay in different forms, that is, native clay, $MnFe_2O_4$/clay composite, and biocomposite. Optimization of pH, Blue XGRRL initial concentration, reaction time, composite dose and temperature was done. The adsorbent and dye solution was mixed in 250 mL capacity conical flasks and placed in an orbital shaking incubator (PA250/25H) at 120 rpm for pre-determined time intervals. The equilibrium adsorption capacity (q_e, mg/g) was measured as shown in Eq. (1).

$$q_e = \frac{\left(C_0 - C_e\right)V}{W} \tag{1}$$

where C_0 is the Blue XGRRL initial concentration (mg/L), C_e is equilibrium Blue XGRRL concentration (mg/L), V and W are volume and adsorbent (g), respectively.

2.5. Adsorption kinetics and equilibrium study

Pseudo-first-order [39], pseudo-second-order [40] and intraparticle diffusion [41] kinetics models and Langmuir [42], Freundlich [43], Temkin [44], Harkins–Jura [45] and Dubinin–Radushkevich [46] isotherms were employed on Blue XGRRL adsorption data on to composites.

2.6. Adsorption thermodynamics

The thermodynamics of Blue XGRRL dye removal was performed in 302 to 337 K under pre-optimized parameters, that is, $\Delta H°$, $\Delta S°$, and $\Delta G°$ were estimated.

2.7. Column study

The adsorption of Blue XGRRL dye onto composites in a continuous system is described in the form of breakthrough curves, which could be defined as the ratio of outlet dye concentration to the inlet dye concentration with respect to time (C_t/C_0 vs. t). $Q_{0.5}$ (breakthrough capacity at 50% or $C_t/C_0 = 0.5$) was deduced as per Eq. (2).

$$\text{Breakthrough capacity} = \frac{\text{Breakthrough time}\left(\text{at } 50\%\right) \times \text{Flow rate X initial dye conc.}}{\text{Mass of the adsorbent in the bed}} \tag{2}$$

3. Results and discussions

3.1. pH effect on adsorption

The initial pH of the dye solution is an imperative factor, which affects the adsorption phenomenon, mainly

adsorption capability. Solution pH alters owing to (1) charge of adsorbent surface (2) adsorbing molecule's degree of ionization (3) degree of dissociation of functional groups present in adsorbent's active sites [33]. The sequestration of Blue XGRRL dye was in 2.0–11 range at 50 mg/L for 120 min. pH effect on adsorption of Blue XGRRL dye is depicted in Fig. 1a. The results revealed highest dye exclusion with native clay, $MnFe_2O_4$/clay composite, and biocomposite was achieved at pH 9, 6 and 8 respectively. The maximum dye removal of Blue XGRRL with $MnFe_2O_4$/clay composite was

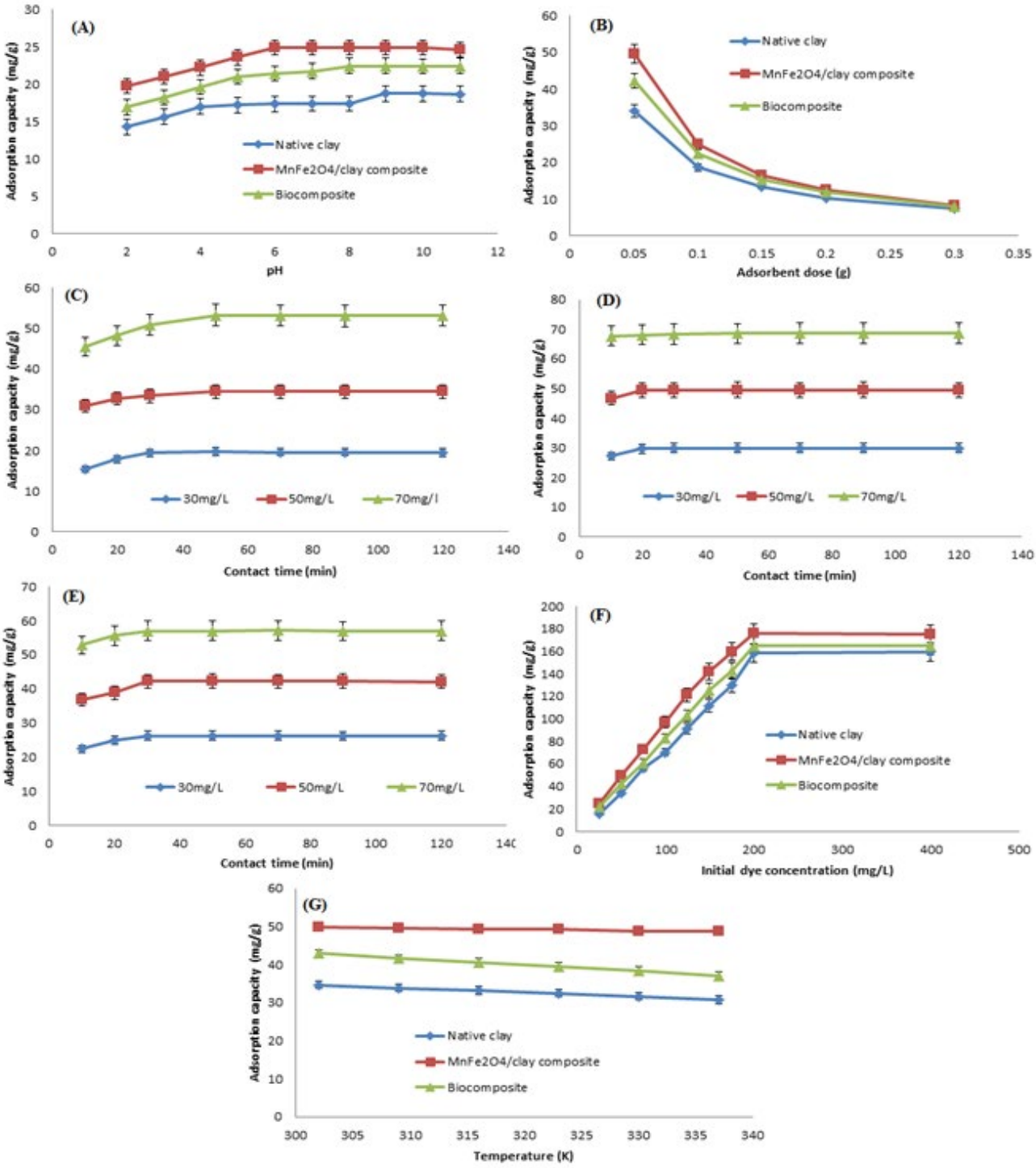

Fig. 1. (a) pH effect on Blue XGRRL dye removal, (b) adsorbent dose effect on Blue XGRRL dye removal, (c) contact time effect on Blue XGRRL dye removal using clay, (d) contact time effect of on Blue XGRRL dye removal using $MnFe_2O_4$/clay composite, (e) contact time effect of on the removal on Blue XGRRL dye removal using biocomposite, (f) initial dye concentration effect on Blue XGRRL dye removal, and (g) temperature effect on Blue XGRRL dye removal.

found to be 24.93. Responses revealed that clay and biocomposite works well in basic pH. Higher pH causes an increase in the amount of OH^- ions increasing cationic dye adsorption capability. In the presence of high acidic conditions, H^+ ions may compete with cations of basic dyes for the occupation of adsorption sites on adsorbent surface hence lowering cationic dye adsorption [47]. Also, the pH of solution change disturbs the surface charge present on the adsorbent. Negative charges produced on surface oxides of adsorbent due to basic medium results in enhanced adsorption of cationic dye [48]. Optimum cationic dye adsorption as a function of pH on different adsorbents was stated by various investigators [49]. In the case of $MnFe_2O_4$/clay composite adsorbent, adsorption at pH 6 cannot be explained well, it is assumed that another type of adsorption, for example, ion exchange, may take place during the adsorption phenomenon of basic dye onto adsorbent [50]. The adsorption process of basic dye on the adsorbent surface might be ascribed to the weak electrostatic interactions that take place among the molecules of dye and the solid surface [51]. Further adsorption study was carried out at an optimum pH value.

3.2. Adsorbent dose effect on adsorption

Dose of adsorbent is of paramount importance for the determination of adsorption capability for a fixed concentration of adsorbate. As the adsorbent dose increased, the adsorption capability of adsorbents was decreased (Fig. 1b). Maximum adsorption capability was observed at 0.05 g/50 mL of dose for all clay and composites. The adsorption decreased with dose as; 34.05 to 7.32 mg/g (clay), 49.57 to 8.32 mg/g ($MnFe_2O_4$/clay composite) 42.24 to 7.94 mg/g (biocomposite). The reduction in adsorption capability can be attributed to aggregation of adsorbent, thus reducing the available surface area for adsorption [52]. Another reason for the reduction in the adsorbed dye amount due to an increase in adsorbent amount might be responsible for the concentration gradient between adsorbent and adsorbate [53].

3.3. Contact time effect on adsorption

The dye adsorption capability was increased as Blue XGRRL dye concentration was increased. The contact time effect was highly significant for the sequestration of Blue XGRRL dye on to composites (Fig. 1c–e). Results revealed that adsorbents possess capabilities for fast dye removal. Dyes were rapidly adsorbed in the beginning and with the passage of time, the adsorption process was slowed down. Equilibrium was achieved in 20–50 min of contact time for all types of adsorbents and beyond this, the adsorption did not change. It may be due to the fact that initially, boundary layer diffusion of the solute molecules takes place due to which high diffusion of molecules takes place into the external face of adsorbent and then, slow diffusion of molecules of the dye takes place to the internal surface [14].

3.4. Initial Blue XGRRL dye concentration effect on adsorption

The Blue XGRRL dye concentration was changed from 25–400 mg/L at optimized conditions and response is depicted in Fig. 1e. As the initial concentration of Blue XGRRL dye was increased, the dye sequestration was also enhanced and so on. This enhancement was attributed to the force of the concentration gradient. The concentration of Blue XGRRL dye in the solution was higher and a gradient was developed between two phases and thus, adsorption was enhanced [15,16]. Hydrophobic interaction between Blue XGRRL dye and composite may also exist [54]. After increasing Blue XGRRL dye concentration from 25–400 mg/L, the sequestration was increased from 15.56–159.4 mg/g (clay), 24.92 to 175 mg/g ($MnFe_2O_4$/clay composite) and 21.61 to 165.1 mg/g (biocomposite) for Blue XGRRL dye.

3.5. Temperature effect on adsorption

The influence of temperature on adsorption kinetics was determined in the range of 302–337 K and the response thus observed is shown in Fig. 1f. The solubility and particularly the chemical potential of adsorbate are greatly affected by temperature [15,16]. The adsorption capability decreased with temperature, which exothermic process. Blue XGRRL dye sequestration was higher at 302 K and low sequestration at elevated temperature might be due to the weakening of adsorptive forces [55]. The temperature may cause more expansion of pores, which may cause leaching of dye molecules which are adsorbed onto the adsorbent surface [56]. The sequestration was reduced from 34.62 to 30.78 mg/g (clay), 49.93 to 48.68 mg/g ($MnFe_2O_4$/clay composite) and 42.92 to 37.03 mg/g (biocomposite) at higher temperature. Previously, acid blue 129 on HCl modified bentonite clay also showed similar behavior [57]. When the temperature was increased from 10°C to 40°C the quantity of dye adsorbed decreased from 7 to 4.2 mol/g.

3.6. Kinetic studies

Pseudo-first-order kinetic model expression is shown in Eq. (3). Where, K_1, q_e, q_t and t are representing rate constant, adsorption capability at equilibrium and time, respectively.

$$\log\left(q_e - q_t\right) = \log q_e - K_1 \times \frac{t}{2.303} \tag{3}$$

The values obtained after adsorption of Blue XGRRL dye by using native clay, $MnFe_2O_4$/clay composite, and biocomposite adsorbents are described in Tables 1–3. Using the Lagergren pseudo-first-order model, a graph between $\log(q_e - q_t)$ and t revealed a low correlation coefficient (R^2) and the small value of q_e as compared to experimental value was observed. So far, the pseudo-first-order kinetic model was unable to explain the Blue XGRRL adsorption.

The pathway of adsorption covering the entire series of interaction time could be successfully described by the pseudo-second-order kinetic model expression is shown in Eq. (4).

$$\left(\frac{t}{q_t}\right) = \frac{1}{K_2 q_e^2} + \frac{t}{q_e} \tag{4}$$

where K_2 (g/mg min) represents the second-order rate constant. The value of q_e (mg/g) and the constant K_2 (g/mg h)

Table 1
Kinetic modeling of Blue XGRRL dye removal using clay

C_0 (mg/L)	30	50	70
Pseudo-first-order K_1 (L/min)	0.032	0.055	0.039
q_e experimental (mg/g)	19.64	34.42	53.58
q_e calculated (mg/g)	2.461	1.161	1.099
R^2	0.644	0.245	0.108
Pseudo-second-order K_2 (g/mg min)	0.028	0.025	0.009
q_e experimental (mg/g)	19.64	34.42	53.58
q_e calculated (mg/g)	20	35.71	55.6
R^2	0.999	0.999	0.999
Intraparticle diffusion K_{pi} (mg/g min$^{1/2}$)	0.426	0.409	0.959
C_i	15.73	30.64	44.26
R^2	0.593	0.728	0.767

Table 2
Kinetic modeling of Blue XGRRL dye removal using $MnFe_2O_4$/clay composite

C_0 (mg/L)	30	50	70
Pseudo-first-order K_1 (L/min)	0.011	0.013	0.110
q_e experimental (mg/g)	29.92	49.57	68.77
q_e calculated (mg/g)	0.2	0.3	5.95
R^2	0.053	0.076	0.667
Pseudo-second-order K_2 (g/mg min)	0.272	0.08	0.065
q_e experimental (mg/g)	29.92	49.57	68.77
q_e calculated (mg/g)	30.3	50	71.4
R^2	1	1	1
Intraparticle diffusion K_{pi} (mg/g min$^{1/2}$)	0.237	0.233	0.137
C_i	27.83	47.51	67.45
R^2	0.431	0.380	0.898

Table 3
Kinetic modeling of Blue XGRRL dye removal using biocomposite

C_0 (mg/L)	30	50	70
Pseudo-first-order K_1 (L/min)	0.027	0.023	0.055
q_e experimental (mg/g)	26.33	42.21	57.07
q_e calculated (mg/g)	0.175	0.006	0.922
R^2	0.072	0.06	0.250
Pseudo-second-order K_2 (g/mg min)	0.034	0.023	0.031
q_e experimental (mg/g)	26.33	42.21	57.07
q_e calculated (mg/g)	27	43.47	58.8
R^2	0.999	0.999	1
Intraparticle diffusion K_{pi} (mg/g min$^{1/2}$)	0.382	0.605	0.417
C_i	22.88	36.72	53.30
R^2	0.545	0.609	0.553

was obtained from the graph between t/q_t vs. t. The K_2, $q_{e,exp}$, $q_{e,cal}$ and R^2 for adsorption of Blue XGRRL are presented in Tables 1–3. It was seen that experimental and q_e values are close with each other, also R^2 values were high for the adsorption of Blue XGRRL dye. Thus, the pseudo-second-order kinetic model explained the XGRRL dye data for clay composite and biocomposite.

The rate-controlling steps may be influenced by intraparticle diffusion, film diffusion or both of them. The intraparticle diffusion was also applied to evaluate the rate-determining step and relation is shown in Eq. (5):

$$q_t = K_{pi} t^{1/2} + C_i \tag{5}$$

where K_{pi} and C_i are representing the rate constant and intercept, respectively. The numerical values of K_{pi}, C_i and R^2 for Blue XGRRL are presented in Tables 1–3. The intraparticle diffusion model infers that the graph obtained by q_t vs. $t^{1/2}$ is linear. If adsorption reaction could be affected by intraparticle diffusion, then a graph between q_t and $t^{1/2}$ is linear and particle diffusion is a rate determine step when a line intersects origin [58]. The lower value of the correlation coefficient (R^2) is indicative of the fact that the adsorption of Blue XGRRL did not follow the intraparticle diffusion kinetic model.

3.7. Isotherm molding

3.7.1. Langmuir isotherm

This isotherm follows the fact that the adsorption phenomenon of solute from liquid solution occurs in the form of monolayer onto the surface comprising an indistinguishable and energetically equivalent amount of binding sites and expression is presented in Eq. (6).

$$\frac{C_e}{q_e} = \frac{1}{q_m b} + \frac{C_e}{q_m} \tag{6}$$

where q_m = maximum adsorption capacity, b is a constant. The numerical values of the Langmuir constants and R^2 for the adsorption of Blue XGRRL dye are depicted in Table 4. The R^2 showed that the Langmuir isotherm explained the dye sequestration well using composite and biocomposite. R_L was calculated using Eq. (7) [59].

$$R_L = \frac{1}{1 + bC_0} \tag{7}$$

where R_L is a dimensionless constant separation feature for an equilibrium factor. C_0 stands for the initial concentration of dye and the value of b denotes Langmuir constant. R_L value is basically an indication of the nature of isotherm that whether it would be favorable ($0 < R_L < 1$), irreversible $R_L = 0$, linear $R_L = 1$ and unfavorable $R_L > 1$. The values of R_L range from 0–1 with any type of adsorbent which is an indication of the fact that adsorption dye occurred favorably on to clay composite and biocomposite (Table 4).

3.7.2. Freundlich isotherm

Freundlich isotherm assumes heterogeneous adsorbent surface and is used to explain multilayered adsorption. It is related to the interaction among the adsorbed

Table 4
Equilibrium modeling of data of Blue XGRRL dye removal

Isotherm models	Blue XGRRL		
	Native clay	$MnFe_2O_4$/clay composite	Biocomposite
	Langmuir		
q_m calculated(mg/g)	190.0	179.20	170.0
q_m experimental (mg/g)	159.39	175.71	165.08
b	0.06	0.625	0.052
R_L	0.25	0.032	0.277
R^2	0.846	0.999	0.986
	Freundlich		
K_F	6.3	66.2	17.5
n	1.4	3.8	1.9
R^2	0.862	0.862	0.750
Temkin			
A	5.5	37.5	1.6
B	49.59	22.34	39.97
R^2	0.742	0.894	0.775
Harkins–Jura			
A	500	–	1,000
B	1.5	–	1
R^2	0.377	0.574	0.505
Dubinin–Radushkevich			
q_m (mg/g)	123.6	126.1	113.1
β (mol^2kJ^{-2})	0.00004	0.000004	0.000004
E ($kJmol^{-1}$)	112.35	0.353	357.14
R^2	0.872	0.783	0.849

molecules and the non-uniform dissemination of sorption heat over an adsorbent surface. Its mathematical form is shown in Eq. (8).

$$\log q_e = \log K_F + \frac{1}{n}\log C_e \tag{8}$$

where K_F and n are representing constants. K_F reveals adsorption capability, n represents the variation from the linearity of adsorption and is utilized to explain the nature of adsorption phenomenon, C_e is Blue XGRRL dye concentration at equilibrium and q_e is adsorption capacity of Blue XGRRL dye [60]. It is considered when n is equal to unity, it means that the adsorption phenomenon is linear whereas n less than unity reveals the fact that adsorption phenomenon occurs through a chemical route; where, n greater than unity is an indication of favorable adsorption [61]. K_F values, R^2 and n for Blue XGRRL dye are shown in Table 4. Smaller R^2 values showed that the Freundlich isotherm model did not fit to the dye adsorption data, while for native clay adsorbent, higher correlation coefficient value as compared to Langmuir R^2 value exhibited good fitting of Freundlich isotherm toward the experimental data of dye.

3.7.3. Temkin isotherm model

Temkin isotherm assumes non-distinguishable spreading of binding energies over different binding sites and mathematical form is shown in Eq. (9).

$$q_e = B\ln A + B\ln C_e \tag{9}$$

where $B = RT/b$, T is the temperature (K), R is a gas constant and b denotes the Temkin constant. A corresponds to equilibrium binding constant and B provides information of the sorption heat. Values of R^2 and constants can be determined via a plot having $\ln C_e$ vs. q_e. R^2 value and other constants are mentioned in Table 4. Low R^2 values reveal that the experimental result for Blue XGRRL dye did not fit to the dye adsorption data on to clay composite and biocomposite in case of Temkin isotherm.

3.7.4. Harkins–Jura isotherm model

This isotherm is based on heterogeneous pore distribution and explained the multilayered adsorption process. Harkins–Jura isotherm linear form is shown Eq. (10). Harkins–Jura's

constant values are depicted in Table 4. The R^2 values for the Blue XGRRL dye adsorption data on to clay composite and biocomposite revealed the unsuitability of this model.

$$\frac{1}{qe^2} = \left(\frac{B}{A}\right) - \left(\frac{1}{A}\right)\log C_e \tag{10}$$

3.7.5. Dubinin–Radushkevich (D–R) model

This model assumes the non-homogenous surface of the adsorbent. It is utilized for the determination of porosity apparent free energy. The D–R isotherm mathematical form is depicted in Eq. (11) [46].

$$\ln q_e = \ln q_m - \beta\varepsilon^2 \tag{11}$$

where β q_m and ε are representing constant, theoretical saturation capacity and Polanyi potential:

$$\varepsilon = RT\ln\left(1+\frac{1}{C_e}\right) \tag{12}$$

where R = gas constant and T = temperature. The mean free energy of adsorption E could be explained as free energy change when 1 mole of ions moved from infinity into solution to the adsorbent. E could be calculated with the help of β value using Eq. (13) [62]. D–R parameter values are expressed in Table 4. Blue XGRRL dye showed better fitness of this model by native clay adsorbent, while it did not explain the dye adsorption data for clay composite and biocomposite.

$$E = \frac{1}{(2\beta)^{1/2}} \tag{13}$$

3.8. Thermodynamic studies

The thermodynamic parameters, that is, ΔS, ΔH, and ΔG were estimated (using Eq. (14), R is a gas constant and T is absolute temperature) for Blue XGRRL dye and values are depicted in Table 5.

$$\ln\left(K_d\right) = \frac{\Delta S^o}{R} - \frac{\Delta H^o}{R}\times\frac{1}{T} \tag{14}$$

Adsorption of Blue XGRRL onto native clay, $MnFe_2O_4$/clay composite, and biocomposite was an exothermic process, as negative value of $\Delta H°$ was observed. $\Delta S°$ values depict a decrease in disorders at solution/solid interface [63]. The negative value of $\Delta G°$ reveals that the adsorption phenomenon was spontaneous in nature and these findings are in line with a previous report [64].

3.9. Influence of electrolytes

The influence of the ionic strength on uptake of Blue XGRRL dye was analyzed by adding different concentrations of electrolyte (ranging from 0.1 to 0.5 M) $AlCl_3{\cdot}6H_2O$, NaCl, $CaCl_2{\cdot}2H_2O$, $KNO_3$and $MgSO_4{\cdot}7H_2O$ in 50 mg/L of dye solution containing 0.05 g/50 mL of $MnFe_2O_4$/clay composite adsorbent. The occurrence of electrolytes in solution reduced the adsorption capacity of dye. The existence of ions may cause vanishing of the electrostatic forces between active binding sites and dye molecules, hence the adsorbed amount reduces when salt concentration increased (Fig. 2a). On the other hand, Safa and Bhatti [65] evaluated the impact of different salts on the adsorption phenomena of dyes via rice husk adsorbent. Various salts ($NaNO_3$, $MgSO_4{\cdot}H_2O$, NH_4NO_3, $CaCl_2{\cdot}2H_2O$, and NaCl) were utilized in a concentration range of 0.01–0.3 M and results revealed that occurrence of the salts boosted biosorption capability of rice husk for adsorptive removal of dyes from their aqueous media.

3.10. Influence of heavy metal ions

The removal efficiency adsorbents are affected by the occurrence of heavy metal ions in medium and in this regard, Cd, Pb, Co, Zn, and Cu effect were studied on Blue XGRRL dye sequestration using composites and the responses thus obtained are depicted in Fig. 2b. Results revealed that adsorption of Blue XGRRL dye was decreased by metal ions, which could possibly be due to competition with adsorbent molecules for the occupation of binding sites of adsorbent of dye molecule and consequently adsorption

Table 5
Thermodynamic parameters for the removal of Blue XGRRL using composite

Temperature (K)	Blue XGRRL								
	Native clay			$MnFe_2O_4$/clay composite			Biocomposite		
	$\Delta G°$	$\Delta H°$	$\Delta S°$	$\Delta G°$	$\Delta H°$	$\Delta S°$	$\Delta G°$	$\Delta H°$	$\Delta S°$
	(kJ/mol)	(kJ/mol)	($Jmol^{-1}$ K^{-1})	(kJ/mol)	(kJ/mol)	($Jmol^{-1}$ K^{-1})	(kJ/mol)	(kJ/mol)	($Jmol^{-1}$ K^{-1})
302	–2.04	–8.09	–20.03	–14.89	–64.78	–165.19	–4.46	–17.47	–43.09
309	–1.90			–13.73			–4.16		
316	–1.76			–12.57			–3.85		
323	–1.62			–11.42			–3.57		
330	–1.48			–10.26			–3.26		
337	–1.34			–9.11			–2.95		

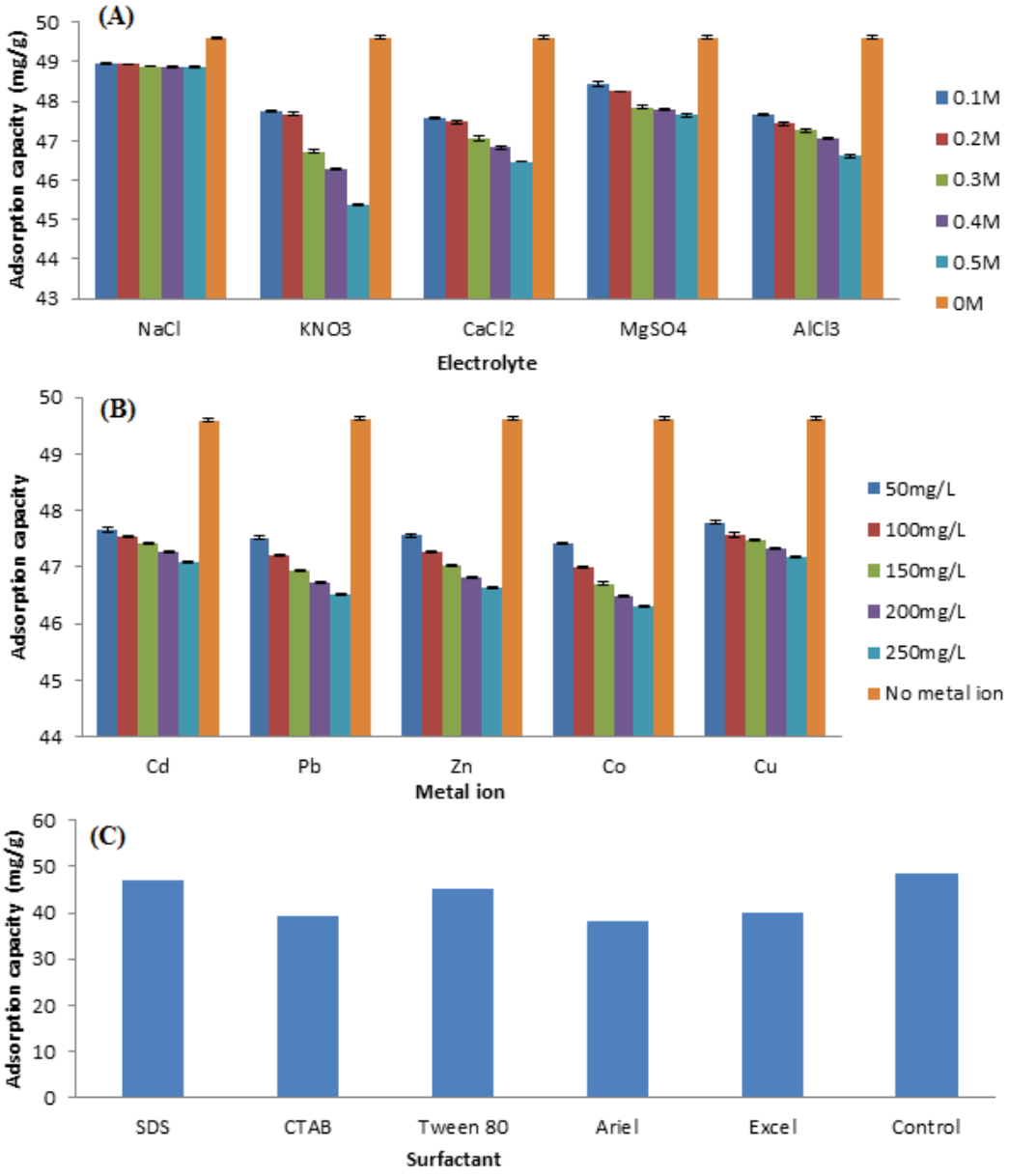

Fig. 2. (a) Electrolytes effect on Blue XGRRL dye removal using of $MnFe_2O_4$/clay composite, (b) heavy metal ions effect on Blue XGRRL dye removal using $MnFe_2O_4$/clay composite, and (c) surfactants/detergents effect on Blue XGRRL dye removal using $MnFe_2O_4$/clay composite.

capability was decreased [66]. Previously, the presence of Cd, Co and Pb increased the biosorption capacity, while Cr and Cu decreased the adsorption potential of the adsorbent for Indosol Black NF dye [55].

3.11. Influence of surfactants/detergents

Various surfactants (CTAB, SDS and Tween 80) and two detergents (Excel and Ariel) were utilized (1%) to determine their impact on the removal of Blue XGRRL dye on to clay composite and biocomposite. The results (Fig. 2c) revealed that surfactants in the dye solution also reduced the adsorption capability of clay composite and biocomposite. This may due to the fact that competition between surfactants and molecules of dye takes place for binding onto adsorbent external [67]. It was also noticed that surfactants reduced the sequestration agro-waste for Turquoise Blue PG dye [68].

3.12. Column study

3.12.1. Influence of bed height

The adsorption of dye in a column is influenced by the amount of adsorbent in column and bed height affect the sequestration of dye in a column adsorption mode and 1

to 3 cm column height was studied at optimum pH, Blue XGRRL dye initial dye concentration and flow rate. The findings (Fig. 3) showed that the bed height affected the dye adsorption. The breakthrough time and adsorption efficiencies observed are depicted in Table 6. When bed height was increased, the dye adsorption was enhanced. It may be because of the accessibility of a greater number of binding sites [69]. Results reveal that with high bed height, breakthrough time also increased and this might be a reduction in axial dispersion of mass transfer that leads to an upsurge in the diffusion of dye molecules. Thus at high bed heights, solute gets adequate time for diffusion into adsorbent and adsorption efficiency may increase. Previously, the influence of bed height was examined by [70] for adsorptive removal of nitrophenol using nano iron oxide and alginate microspheres. It was observed that when bed height was increased from 2.5–10 cm, the adsorptive removal was also enhanced from 46.6% to 62.2%. Chen [71] also investigated the impact of bed height in column mode on the adsorptive removal of fluoride using Kanuma mud at three-bed heights, that is, 5, 10, and 15 cm. The breakthrough time was influenced by a change in bed height. Sharper breakthrough curves were obtained using smaller bed depth. The breakthrough time was observed to be decreased when bed depth was decreased from 15 to 5 cm because binding sites become constrained at smaller bed height.

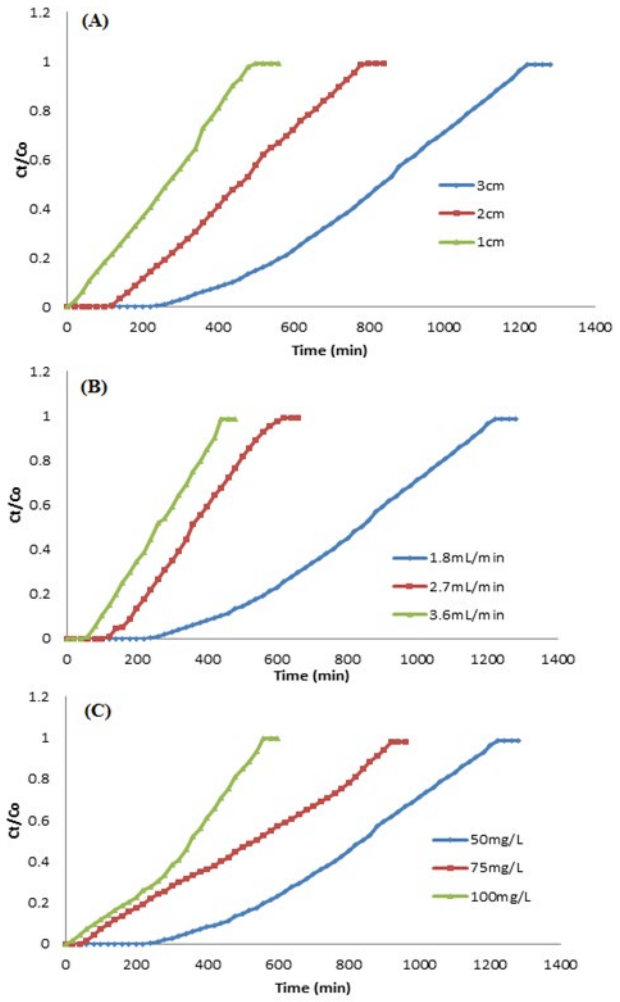

Fig. 3. Blue XGRRL dye removal as a function of (a) bed height, (b) flow rate, and (c) Blue XGRRL dye initial concentration.

3.12.2. Influence of flow rate

Flow rates in the range of 1.8–3.6 mL/min were studied and the breakthrough curve for a column was obtained from plot C_t/C_0 (C_t and C_0 vs. time and response are shown in Fig. 3. The column was observed to perform well during the lowest flow rate (1.8 mL/min). Also, the time was reduced from 830 to 250 min for Blue XGRRL when the flow rate increased 1.8–3.6 mL/min. At higher flow rates, dye ions could not get adequate time for diffusion inside the pores of clay composite and left the column before reaching steadiness. As(II) sequestration using modified calcined bauxite [50] and dye on surfactant-modified zeolite also revealed similar adsorption trends [51].

3.12.3. Influence of initial dye concentration

The Blue XGRRL dye initial concentrations were varied and other conditions kept constant and responses thus obtained are depicted in Fig. 3. The time required for attaining a 50% breakthrough capacity reduced when initial dye concentration was increased. It may be due to low concentration slope that causes sluggish transport owing to lessened diffusion coefficient and a lessened mass transfer coefficient. Adsorption capability of adsorbents was observed to be increased when initial concentration was increased. The enhancement in dye removal when the initial concentration of dye was increased that could be due to the concentration difference in Blue XGRRL dye in medium and on the surface of the composite [72]. Adsorption capability of the selected adsorbent achieved from the column study was less than that of attained from the batch mode of study using the same initial Blue XGRRL dye concentration. The difference among adsorption capacity of adsorbents in continuous and batch mode experiments might be due to the reason that the active surface area of adsorbents. In continuous column mode, the molecules of dye and adsorbent do not find sufficient time of contact resulting in lower adsorption capacity [73]. Nawaz [74] determined the impact of the initial concentration of dye on adsorptive removal of Novacron Golden Yellow dye using agricultural waste in the column mode experiments as a function of the initial concentration of dye. Results showed that breakthrough time reduced by increasing the initial concentration.

3.12.4. Thomas model

This model is established on factors that second-order reversible reaction kinetics is followed by the rate governing force and model the adsorption in packed systems. The linear form of the Thomas model is shown in Eq. (15).

$$\ln\left(\frac{C_0}{C_t}\right)=\frac{K_{\mathrm{Th}}\times q_0\times W}{Q}-K_{\mathrm{Th}}\times C_0\times t \tag{15}$$

where q_0 = dye uptake, k_{Th} = rate constant; Q = flow rate; C_0 = inlet dye concentration; C_t = outlet concentration at time t; t_{total} = flow time, W = adsorbent mass utilized in column. A linear graph of $\ln[(C_0/C_t)-1]$ and time (t) was drawn for the determination of values of k_{Th} and q_0 values. Obtained data for Blue XGRRL dye was fitted to the Thomas model (Table 6). k_{Th} values expressed a linear increase by increasing the flow rate.

3.12.5. Bed depth service time (BDST) model

The bed depth service time (BDST) model basically follows the equation of Bohart–Adams. A selected breakthrough point can be obtained by applying this model since it gives an idea of column efficacy. The predicted breakthrough time during which the used adsorbent possesses the aptitude to withstand the adsorptive removal process of a fixed quantity of pollutants before revival is the main designing of column adsorption mode. This precise duration is recognized as the service time of bed. A linear relationship between bed height and time was proposed by Hutchins and is expressed in Eq. (16).

$$t = \frac{N_0 Z}{C_0 U} - \frac{1}{K_a C_0} \ln\left(\frac{C_0}{C_b} - 1\right) \tag{16}$$

where C_0 = Blue XGRRL dye initial concentration, C_b = breakthrough, k_a = rate constant, U = linear velocity, N_0 = adsorption efficiency, Z = bed height and t = time. The C_t/C_0 ratio, R^2 are higher that demonstrate better agreement of the experimental dye adsorption data with BDST model (Table 7).

3.13. Characterization of adsorbents

The clay used for the preparation of a composite was characterized for its composition and silica, alumina and other metal oxides obtained was recorded in the clay samples (Table 8). A Fourier-transform infrared spectroscopy spectrum of the clay and $MnFe_2O_4$/clay composite before and after Blue XGRRL dye removal revealed various absorption peaks due to the presence of different functional groups. The peak at 2,300 cm^{-1} was due to N–H bond, whereas 3,700 cm^{-1} peak was due the O–H stretching vibrations and at 1,421.5 cm^{-1} absorption band was due to CH_2 bending. Peak at 850 cm^{-1} was assigned to C–H stretching vibration and 1,501.18 cm^{-1} peak was correlated with a benzene ring. The quartz peak was recorded at 781.17 cm^{-1}. The Si–O–Si peak was observed at 900 cm^{-1}. The X-ray diffraction analysis of clay and composite revealed the existence of the silica and alumina as main constituents and sodium, magnesium, iron, potassium and calcium oxides were minor constituents. It has been reported that clay structure is porous, has high cationic exchangeability and has a high surface area, which offers excellent adsorption properties for different pollutants. Results of present investigation also revealed that clay showed promising efficiency for dye sequestration and clay composite with $MnFe_2O_4$ also enhanced the adsorption

Table 8
Chemical analysis of clay used for composite preparation

Silicon dioxide	61.64
Aluminium oxide	9.8
Ferric oxide	6.23
Calcium oxide	1.94
Magnesium oxide	2.04
Potassium oxide	3.00
Sodium oxide	1.71
Sulfur trioxide	0.529
Cl	0.187

Table 6
Thomas model parameters of Blue XGRRL dye removal

Inlet concentration (mg/L)	Bed height (cm)	Flow rate (mL/min)	k_{Th} (mL/min mg) × 10^3	q_0 (mg/g)	R^2
50	1	1.8	0.14	15.48	0.879
50	2	1.8	0.12	18.10	0.797
50	3	1.8	0.10	23.29	0.943
50	3	2.7	0.28	20.40	0.958
50	3	3.6	0.34	17.70	0.915
75	3	1.8	0.09	25.83	0.914
100	3	1.8	0.08	27.62	0.887

Table 7
BDST parameters of Blue XGRRL dye removal

C_t/C_0	A	B	K_a (L mg^{-1} min^{-1})	N_0 (mg L^{-1})	R^2
0.2	230	7,172.13	0.0000976	4,218	0.970
0.4	270	90.90	0.000088	4,951	0.964
0.6	300	23.39	–0.000342	5,502	0.964

capability of clay, which is an indication that inorganic moieties [75–78] are efficient to enhance the adsorption efficiency of clay and under the current scenario of pollution [79–85], there is need to prepare and utilize the efficient materials for wastewater remediation [2,31,47].

4. Conclusions

Clay composite and biocomposite were prepared and employed for the adsorption of Blue XGRRL dye. Results revealed that basic dye can be proficiently removed using clay composite. The basic pH, low adsorbent dose and low temperature were favorable conditions for dye adsorption. Among native clay, clay composite and biocomposite, the clay composite showed maximum dye removal efficiency of 49.93 mg/g. Langmuir isotherm and pseudo-second-order kinetic model fitted well to the dye adsorption data. The thermodynamic study revealed that the dye adsorption was feasible at lower temperatures and the process was exothermic. Column study results revealed that higher bed heights, low flow rates, and higher initial dye concentrations were feasible conditions for maximum dye removal. In view of promising efficiency, the clay composite could possibly be used for dyes removal from textile wastewater.

Acknowledgement

This work is a part of Ph. D thesis of Miss Sana Nausheen. The authors are thankful to the Higher Education Commission (HEC) of Pakistan for financial assistance under the Indigenous Ph.D. Fellowship Program.

References

[1] N.E. Ibisi, C.A. Asoluka, Use of agro-waste (*Musa paradisiaca* peels) as a sustainable biosorbent for toxic metal ions removal from contaminated water, Chem. Int., 4 (2018) 52–59.
[2] S. Mansouri, N. Elhammoudi, S. Aboul-hrouz, M. Mouiya, L. Makouki, A. Chham, A. Abourriche, H. Hannache, M. Oumam, Elaboration of novel adsorbent from Moroccan oil shale using Plackett–Burman design, Chem. Int., 4 (2018) 7–14.
[3] M. Iqbal, M. Abbas, J. Nisar, A. Nazir, Bioassays based on higher plants as excellent dosimeters for ecotoxicity monitoring: a review, Chem. Int., 5 (2019) 1–80.
[4] A.M. Alkherraz, A.K. Ali, K.M. Elsherif, Removal of Pb(II), Zn(II), Cu(II) and Cd(II) from aqueous solutions by adsorption onto olive branches activated carbon: equilibrium and thermodynamic studies, Chem. Int., 6 (2020) 11–20.
[5] S. Velanganni, A. Manikandan, J.J. Prince, C.N. Mohan, R. Thiruneelakandan, Nanostructured ZnO coated Bi_2S_3 thin films: enhanced photocatalytic degradation of methylene blue dye, Phys. B. Condens. Matter, 545 (2018) 383–389.
[6] G. Mathubala, A. Manikandan, S.A. Antony, P. Ramar, Photocatalytic degradation of methylene blue dye and magneto-optical studies of magnetically recyclable spinel $Ni_xMn_{1-x}Fe_2O_4$ (x = 0.0–1.0) nanoparticles, J. Mol. Struct., 1113 (2016) 79–87.
[7] G. Padmapriya, A. Manikandan, V. Krishnasamy, S.K. Jaganathan, S.A. Antony, Spinel $Ni_xZn_{1-x}Fe_2O_4$ ($0.0 \le x \le 1.0$) nano-photocatalysts: synthesis, characterization and photocatalytic degradation of methylene blue dye, J. Mol. Struct., 1119 (2016) 39–47.
[8] A. Manikandan, A. Saravanan, S.A. Antony, M. Bououdina, One-pot low temperature synthesis and characterization studies of nanocrystalline α-Fe_2O_3 based dye sensitized solar cells, J. Nanosci. Nanotechnol., 15 (2015) 4358–4366.
[9] M. Bilal, M. Iqbal, H. Hu, X. Zhang, Mutagenicity and cytotoxicity assessment of biodegraded textile effluent by Ca-alginate encapsulated manganese peroxidase, Biochem. Eng. J., 109 (2016) 153–161.
[10] A. Babarinde, K. Ogundipe, K.T. Sangosanya, B.D. Akintola, A.-O. Elizabeth Hassan, Comparative study on the biosorption of Pb(II), Cd(II) and Zn(II) using Lemon grass (*Cymbopogon citratus*): kinetics, isotherms and thermodynamics, Chem. Int., 2 (2016) 89–102.
[11] A. Babarinde, G.O. Onyiaocha, Equilibrium sorption of divalent metal ions onto groundnut (*Arachis hypogaea*) shell: kinetics, isotherm and thermodynamics, Chem. Int., 2 (2016) 37–46.
[12] N.K. Benabdallah, D. Harrache, A. Mir, M. de la Guardia, F.-Z. Benhachem, Bioaccumulation of trace metals by red alga *Corallina elongata* in the coast of Beni Saf, west coast, Algeria, Chem. Int., 3 (2017) 220–231.
[13] A. Rashid, H.N. Bhatti, M. Iqbal, S. Noreen, Fungal biomass composite with bentonite efficiency for nickel and zinc adsorption: a mechanistic study, Ecol. Eng., 91 (2016) 459–471.
[14] S. Shoukat, H.N. Bhatti, M. Iqbal, S. Noreen, Mango stone biocomposite preparation and application for crystal violet adsorption: a mechanistic study, Microporous Mesoporous Mater., 239 (2017) 180–189.
[15] M.A. Tahir, H.N. Bhatti, M. Iqbal, Solar Red and Brittle Blue direct dyes adsorption onto *Eucalyptus angophoroides* bark: equilibrium, kinetics and thermodynamic studies, J. Environ. Chem. Eng., 4 (2016) 2431–2439.
[16] N. Tahir, H.N. Bhatti, M. Iqbal, S. Noreen, Biopolymers composites with peanut hull waste biomass and application for Crystal Violet adsorption, Int. J. Biol. Macromol., 94 (2016) 210–220.
[17] R. Bomila, S. Srinivasan, S. Gunasekaran, A. Manikandan, Enhanced photocatalytic degradation of methylene blue dye, opto-magnetic and antibacterial behaviour of pure and La-doped ZnO nanoparticles, J. Supercond. Novel Magn., 31 (2018) 855–864.
[18] G. Mathubala, A. Manikandan, S. Arul Antony, P. Ramar, Enhanced photocatalytic activity of spinel $Cu_xMn_{1-x}Fe_2O_4$ nanocatalysts for the degradation of methylene blue dye and opto-magnetic properties, Nanosci. Nanotechnol. Lett., 8 (2016) 375–381.
[19] A. Manikandan, J.J. Vijaya, S. Narayanan, L.J. Kennedy, Comparative investigation of structural, optical properties and dye-sensitized solar cell applications of ZnO nanostructures, J. Nanosci. Nanotechnol., 14 (2014) 2507–2514.
[20] P. Thilagavathi, A. Manikandan, S. Sujatha, S.K. Jaganathan, S. Arul Antony, sol–gel synthesis and characterization studies of $NiMoO_4$ nanostructures for photocatalytic degradation of methylene blue dye, Nanosci. Nanotechnol. Lett., 8 (2016) 438–443.
[21] A. Manikandan, J.J. Vijaya, C. Ragupathi, L.J. Kennedy, Optical properties and dye-sensitized solar cell applications of ZnO Nanostructures prepared by microwave combustion synthesis, J. Nanosci. Nanotechnol., 14 (2014) 2584–2590.
[22] M. Shabandokht, E. Binaeian, H.-A. Tayebi, Adsorption of food dye Acid red 18 onto polyaniline-modified rice husk composite: isotherm and kinetic analysis, Desal. Wat. Treat., 57 (2016) 27638–27650.
[23] R.R. Gonte, G. Shelar, K. Balasubramanian, Polymer–agro-waste composites for removal of Congo red dye from wastewater: adsorption isotherms and kinetics, Desal. Wat. Treat., 52 (2014) 7797–7811.
[24] R. Rezaei Kalantry, A. Jonidi Jafari, A. Esrafili, B. Kakavandi, A. Gholizadeh, A. Azari, Optimization and evaluation of reactive dye adsorption on magnetic composite of activated carbon and iron oxide, Desal. Wat. Treat., 57 (2016) 6411–6422.
[25] S. Giri, P. Sahoo, R. Das, N. Das, Coke/Fe_3O_4 nanoparticle composites: synthesis, characterization and adsorption behaviour towards organic dyes, Desal. Wat. Treat., 57 (2016) 17483–17493.
[26] T. Hiwot, Mango (*Magnifera indica*) seed oil grown in Dilla town as potential raw material for biodiesel production using NaOH-a homogeneous catalyst, Chem. Int., 4 (2018) 198–205.
[27] Q. Manzoor, R. Nadeem, M. Iqbal, R. Saeed, T.M. Ansari, Organic acids pretreatment effect on *Rosa bourbonia* phyto-biomass for

removal of Pb(II) and Cu(II) from aqueous media, Bioresour. Technol., 132 (2013) 446–452.
[28] M. Mushtaq, H.N. Bhatti, M. Iqbal, S. Noreen, Eriobotrya japonica seed biocomposite efficiency for copper adsorption: isotherms, kinetics, thermodynamic and desorption studies, J. Environ. Manage., 176 (2016) 21–33.
[29] R. Nadeem, Q. Manzoor, M. Iqbal, J. Nisar, Biosorption of Pb(II) onto immobilized and native *Mangifera indica* waste biomass, J. Ind. Eng. Chem., 35 (2016) 185–194.
[30] H. Naeem, H.N. Bhatti, S. Sadaf, M. Iqbal, Uranium remediation using modified *Vigna radiata* waste biomass, Appl. Radiat. Isot., 123 (2017) 94–101.
[31] A. Chham, E. Khouya, M. Oumam, A.K. Abourriche, S. Gmouh, M. larzek, S. Mansouri, N. Elhammoudi, N. Hanafi, H. Hannache, The use of insoluble mater of Moroccan oil shale for removal of dyes from aqueous solution, Chem. Int., 4 (2018) 67–76.
[32] T.N. Chikwe, R.E. Ekpo, I. Okoye, Competitive adsorption of organic solvents using modified and unmodified calcium bentonite clay mineral, Chem. Int., 4 (2018) 230–239.
[33] S. Ghezali, A. Mahdad-Benzerdjeb, M. Ameri, A.Z. Bouyakoub, Adsorption of 2,4,6-trichlorophenol on bentonite modified with benzyldimethyltetradecylammonium chloride, Chem. Int., 4 (2018) 24–32.
[34] A. Kausar, M. Iqbal, A. Javed, K. Aftab, Z.-i.-H. Nazli, H.N. Bhatti, S. Nouren, Dyes adsorption using clay and modified clay: a review, J. Mol. Liq., 256 (2018) 395–407.
[35] O. Chidi, R. Kelvin, Surface interaction of sweet potato peels (*Ipomoea batata*) with Cd(II) and Pb(II) ions in aqueous medium, Chem. Int., 4 (2018) 221–229.
[36] M. Fazal-ur-Rehman, Methodological trends in preparation of activated carbon from local sources and their impacts on production: a review, Chem. Int., 4 (2018) 109–119.
[37] I. Ullah, R. Nadeem, M. Iqbal, Q. Manzoor, Biosorption of chromium onto native and immobilized sugarcane bagasse waste biomass, Ecol. Eng., 60 (2013) 99–107.
[38] S. Hashemian, $MnFe_2O_4$/bentonite nano composite as a novel magnetic material for adsorption of acid red 138, Afr. J. Biotechnol., 9 (2010) 8667–8671.
[39] S. Lagergren, About the theory of so-called adsorption of soluble substances, Kungliga Svenska Vetenskapsakademiens Handlingar, 24 (1898) 1–39.
[40] Y. Ho, G. McKay, D. Wase, C. Forster, Study of the sorption of divalent metal ions on to peat, Adsorpt. Sci. Technol., 18 (2000) 639–650.
[41] W.J. Weber, J.C. Morris, Kinetics of adsorption on carbon from solution, J. Sanit. Eng. Div., 89 (1963) 31–60.
[42] I. Langmuir, The adsorption of gases on plane surfaces of glass, mica and platinum, J. Am. Chem. Soc., 40 (1918) 1361–1403.
[43] H. Freundlich, Over the adsorption in solution, J. Phys. Chem., 57 (1906) 1100–1107.
[44] M. Temkin, V. Pyzhev, Kinetics of ammonia synthesis on promoted iron catalysts, Acta Physiochim., URSS, 12 (1940) 217–222.
[45] W.D. Harkins, G. Jura, Surfaces of solids. XIII. A vapor adsorption method for the determination of the area of a solid without the assumption of a molecular area, and the areas occupied by nitrogen and other molecules on the surface of a solid, J. Am. Chem. Soc., 66 (1944) 1366–1373.
[46] M. Dubinin, L. Raduskhevich, Proceedings of the Academy of Sciences of the USSR, Phys. Chem., 55 (1947) 327–329.
[47] M. Laissaoui, Y. Elbatal, I. Vioque, G. Manjon, Adsorption of methylene blue on bituminous schists from Tarfaya-Boujdour, Chem. Int., 3 (2017) 343–352.
[48] C.K. Lee, K.S. Low, S. Chow, Chrome sludge as an adsorbent for colour removal, Environ. Technol., 17 (1996) 1023–1028.
[49] S. Wang, Z. Zhu, A. Coomes, F. Haghseresht, G. Lu, The physical and surface chemical characteristics of activated carbons and the adsorption of methylene blue from wastewater, J. Colloid Interface Sci., 284 (2005) 440–446.
[50] P. Bhakat, A. Gupta, S. Ayoob, Feasibility analysis of As(III) removal in a continuous flow fixed bed system by modified calcined bauxite (MCB), J. Hazard. Mater., 139 (2007) 286–292.
[51] O. Ozdemir, M. Turan, A.Z. Turan, A. Faki, A.B. Engin, Feasibility analysis of color removal from textile dyeing wastewater in a fixed-bed column system by surfactant-modified zeolite (SMZ), J. Hazard. Mater., 166 (2009) 647–654.
[52] K. Legrouri, E. Khouya, H. Hannache, M. El Hartti, M. Ezzine, R. Naslain, Activated carbon from molasses efficiency for Cr(VI), Pb(II) and Cu(II) adsorption: a mechanistic study, Chem. Int., 3 (2017) 301–310.
[53] K.D. Ogundipe, A. Babarinde, Comparative study on batch equilibrium biosorption of Cd(II), Pb(II) and Zn(II) using plantain (*Musa paradisiaca*) flower: kinetics, isotherm, and thermodynamics, Chem. Int., 3 (2017) 135–149.
[54] H. Zhu, M. Zhang, Y. Liu, L. Zhang, R. Han, Study of congo red adsorption onto chitosan coated magnetic iron oxide in batch mode, Desal. Wat. Treat., 37 (2012) 46–54.
[55] S. Sadaf, H.N. Bhatti, Batch and fixed bed column studies for the removal of Indosol Yellow BG dye by peanut husk, J. Taiwan Inst. Chem. Eng., 45 (2014) 541–553.
[56] S. Khattri, M. Singh, Use of Sagaun sawdust as an adsorbent for the removal of crystal violet dye from simulated wastewater, Environ. Prog. Sustainable Energy, 31 (2012) 435–442.
[57] Z. Ullah, S. Hussain, S. Gul, S. Khan, F. Bangash, Use of HCl-modified bentonite clay for the adsorption of Acid Blue 129 from aqueous solutions, Desal. Wat. Treat., 57 (2016) 8894–8903.
[58] S.H. Kareem, A. Enaas, Adsorption of Congo, Red rhodamine B and disperse blue dyes from aqueous solution onto raw flint clay, Baghdad, Sci. J., 9 (2012) 680–688.
[59] K. Hall, L. Eagleton, A. Acrivos, T. Vermeulen, Pore-and solid-diffusion kinetics in fixed-bed adsorption under constant-pattern conditions, Ind. Eng. Chem. Fundam., 5 (1966) 212–223.
[60] F. Arias, T.K. Sen, Removal of zinc metal ion (Zn^{2+}) from its aqueous solution by kaolin clay mineral: a kinetic and equilibrium study, Colloids Surf., A, 348 (2009) 100–108.
[61] M.A.M. Salleh, D.K. Mahmoud, W.A.W.A. Karim, A. Idris, Cationic and anionic dye adsorption by agricultural solid wastes: a comprehensive review, Desalination, 280 (2011) 1–13.
[62] S. Kundu, A. Gupta, Adsorptive removal of As(III) from aqueous solution using iron oxide coated cement (IOCC): evaluation of kinetic, equilibrium and thermodynamic models, Sep. Purif. Technol., 51 (2006) 165–172.
[63] A. Mittal, J. Mittal, A. Malviya, V. Gupta, Removal and recovery of Chrysoidine Y from aqueous solutions by waste materials, J. Colloid Interface Sci., 344 (2010) 497–507.
[64] F. Deniz, S.D. Saygideger, Removal of a hazardous azo dye (Basic Red 46) from aqueous solution by princess tree leaf, Desalination, 268 (2011) 6–11.
[65] Y. Safa, H.N. Bhatti, Adsorptive removal of direct dyes by low cost rice husk: Effect of treatments and modifications, Afr. J. Biotechnol., 10 (2011) 3128–3142.
[66] M. Asgher, H.N. Bhatti, Evaluation of thermodynamics and effect of chemical treatments on sorption potential of Citrus waste biomass for removal of anionic dyes from aqueous solutions, Ecol. Eng., 38 (2012) 79–85.
[67] I.U. Haq, H.N. Bhatti, M. Asgher, Removal of Solar Red BA textile dye from aqueous solution by low cost barley husk: equilibrium, kinetic and thermodynamic study, Can. J. Chem. Eng., 89 (2011) 593–600.
[68] H.N. Bhatti, S. Nausheen, Equilibrium and kinetic modeling for the removal of Turquoise Blue PG dye from aqueous solution by a low-cost agro waste, Desal. Wat. Treat., 55 (2015) 1934–1944.
[69] Y. Al-Degs, M. Khraisheh, S. Allen, M. Ahmad, Adsorption characteristics of reactive dyes in columns of activated carbon, J. Hazard. Mater., 165 (2009) 944–949.
[70] A. Soni, A. Tiwari, A. Bajpai, Adsorption of o-nitrophenol onto nano iron oxide and alginate microspheres: batch and column studies, Afr. J. Pure Appl. Chem., 6 (2012) 161–173.
[71] N. Chen, Z. Zhang, C. Feng, M. Li, R. Chen, N. Sugiura, Investigations on the batch and fixed-bed column performance of fluoride adsorption by Kanuma mud, Desalination, 268 (2011) 76–82.
[72] Z. Aksu, F. Gönen, Biosorption of phenol by immobilized activated sludge in a continuous packed bed: prediction of breakthrough curves, Process. Biochem., 39 (2004) 599–613.

[73] Z. Al-Qodah, W. Lafi, Continuous adsorption of acid dyes in fixed beds, J. Water Supply, 52 (2003) 189–198.
[74] S. Nawaz, H.N. Bhatti, T.H. Bokhari, S. Sadaf, Removal of Novacron Golden Yellow dye from aqueous solutions by low-cost agricultural waste: batch and fixed bed study, Chem. Ecol., 30 (2014) 52–65.
[75] A. Mary Jacintha, A. Manikandan, K. Chinnaraj, S. Arul Antony, P. Neeraja, Comparative studies of spinel $MnFe_2O_4$ nanostructures: structural, morphological, optical, magnetic and catalytic properties, J. Nanosci. Nanotechnol., 15 (2015) 9732–9740.
[76] A. Silambarasu, A. Manikandan, K. Balakrishnan, S.K. Jaganathan, E. Manikandan, J.S. Aanand, Comparative study of structural, morphological, magneto-optical and photo-catalytic properties of magnetically reusable spinel $MnFe_2O_4$ nanocatalysts, J. Nanosci. Nanotechnol., 18 (2018) 3523–3531.
[77] A. Manikandan, M. Durka, K. Seevakan, S.A. Antony, A novel one-pot combustion synthesis and opto-magnetic properties of magnetically separable spinel $Mn_xMg_{1-x}Fe_2O_4$ ($0.0 \le x \le 0.5$) nanophotocatalysts, J. Supercond. Novel Magn., 28 (2015) 1405–1416.
[78] A. Manikandan, M. Durka, S.A. Antony, A novel synthesis, structural, morphological, and opto-magnetic characterizations of magnetically separable spinel $Co_xMn_{1-x}Fe_2O_4$ ($0 \le x \le 1$) nanocatalysts, J. Supercond. Novel Magn., 27 (2014) 2841–2857.
[79] A. Silambarasu, A. Manikandan, K. Balakrishnan, Room-temperature superparamagnetism and enhanced photocatalytic activity of magnetically reusable spinel $ZnFe_2O_4$ nanocatalysts, J. Supercond. Novel Magn., 30 (2017) 2631–2640.
[80] H. Bakhshi, A. Darvishi, Preparation and evaluation of hydrogel composites based on starch-g-PNaMA/eggshell particles as dye biosorbent, Desal. Wat. Treat., 57 (2016) 18144–18156.
[81] W. Cui, K. Zhao, J. Wei, G. Cheng, H. Li, L. Sui, S. Li, Adsorption properties of dye imprinted polysiloxane composite microspheres using strong basic anion-exchange resin as matrix, Desal. Wat. Treat., 51 (2013) 7604–7611.
[82] A. Ebrahimi, E. Pajootan, M. Arami, H. Bahrami, Optimization, kinetics, equilibrium, and thermodynamic investigation of cationic dye adsorption on the fish bone, Desal. Wat. Treat., 53 (2015) 2249–2259.
[83] M. Sasmaz, B. Akgül, D. Yıldırım, A. Sasmaz, Mercury uptake and phytotoxicity in terrestrial plants grown naturally in the Gumuskoy (Kutahya) mining area, Turkey, Int. J. Phytorem., 18 (2016) 69–76.
[84] P. Sharma, D.J. Borah, P. Das, M.R. Das, Cationic and anionic dye removal from aqueous solution using montmorillonite clay: evaluation of adsorption parameters and mechanism, Desal. Wat. Treat., 57 (2016) 8372–8388.
[85] E.I. Unuabonah, A.O. Adedapo, C.O. Nnamdi, A. Adewuyi, M.O. Omorogie, K.O. Adebowale, B.I. Olu-Owolabi, A.E. Ofomaja, A. Taubert, Successful scale-up performance of a novel papaya-clay combo adsorbent: up-flow adsorption of a basic dye, Desal. Wat. Treat., 56 (2015) 536–551.